

Multicentennial-scale hydrological changes in the Black Sea and northern Red Sea during the Holocene and the Arctic/North Atlantic Oscillation

Frank Lamy,¹ Helge W. Arz,¹ Gérard C. Bond,² André Bahr,³ and Jürgen Pätzold³

Received 3 June 2005; revised 20 September 2005; accepted 4 November 2005; published 21 February 2006.

[1] Paleoenvironmental proxy data for ocean properties, eolian sediment input, and continental rainfall based on high-resolution analyses of sediment cores from the southwestern Black Sea and the northernmost Gulf of Aqaba were used to infer hydroclimatic changes in northern Anatolia and the northern Red Sea region during the last ~7500 years. Pronounced and coherent multicentennial variations in these records reveal patterns that strongly resemble modern temperature and rainfall anomalies related to the Arctic Oscillation/North Atlantic Oscillation (AO/NAO). These patterns suggest a prominent role of AO/NAO-like atmospheric variability during the Holocene beyond interannual to interdecadal timescales, most likely originating from solar output changes.

Citation: Lamy, F., H. W. Arz, G. C. Bond, A. Bahr, and J. Pätzold (2006), Multicentennial-scale hydrological changes in the Black Sea and northern Red Sea during the Holocene and the Arctic/North Atlantic Oscillation, *Paleoceanography*, 21, PA1008, doi:10.1029/2005PA001184.

1. Introduction

[2] It is now well accepted that the Arctic Oscillation/North Atlantic Oscillation (AO/NAO), the Northern Hemisphere's dominant mode of atmospheric variability at interannual to interdecadal timescales, exerts a strong influence on middle- and high-latitude continental climate [Hurrell, 1995; Thompson and Wallace, 2001]. These changes are particularly evident around the North Atlantic but also considerably affect climates of remote regions, such as Turkey and the Middle East [Cullen and deMenocal, 2000; Felis et al., 2004; Turkes and Erlat, 2003]. In order to improve our understanding of natural AO/NAO variations at multicentennial timescales in relation to the potential impact of human activities, it is crucial to investigate the long-term behavior of this atmospheric mode during the present warm climate stage, the Holocene. AO/NAO reconstructions based on instrumental, historical, and different climate proxy data from, for example, tree rings and ice cores only reach back to the past millennium and give insight into interannual- to interdecadal-scale variability [Cook et al., 2002; Cullen et al., 2001; Luterbacher et al., 2001]. On longer timescales, only a few sedimentological and geochemical proxy records have been interpreted in relation to AO/NAO changes. Keigwin and Pickart [1999] provided, for example, evidence of antiphase SST changes north and south of the Gulf Stream during the last 2000

years that are similar to SST anomalies related to the modern AO/NAO. Noren et al. [2002] showed that variations in New England storminess may reflect millennial-scale changes in the preferred phase of the AO during the Holocene. A comparison of drift ice variations with temperature changes in Europe, Greenland, and the subtropical North Atlantic suggests, on the other hand, basin-wide uniform changes on multicentennial to millennial timescales distinct from the modern AO/NAO anomaly pattern [Bond et al., 2001].

[3] Two sensitive regions where modern AO/NAO changes at interannual to interdecadal timescales result in large hydrological impacts and which are also suitable for long-term climate reconstructions are Turkey and the Middle East (Figure 1) [Cullen and deMenocal, 2000; Felis et al., 2004; Turkes and Erlat, 2003]. Here we present a comparison of paleoenvironmental proxy data for ocean properties, eolian sediment input, and continental rainfall based on high-resolution analyses of sediment cores from the southwestern Black Sea and the northernmost Gulf of Aqaba. These proxy records of hydroclimatic changes in northern Anatolia and the northern Red Sea region show multicentennial-scale variations during the last ~7500 years that strongly resemble modern AO/NAO-related temperature and rainfall anomalies, suggesting a prominent role of the AO/NAO during the Holocene not only at interannual to interdecadal timescales.

2. Study Areas

2.1. Black Sea

[4] We focus on two sediment cores from the Anatolian continental slope in the southwestern Black Sea, GeoB 7622-2 (41°32.1'N, 31°10.1'E, 1305 m water depth) and GeoB 7625-2 (41°26.7'N, 31°04.0'E, 1242 m water depth) (Figure 1). The two coring sites are located ~65 and ~50 km northeast of the Sakarya River mouth on topo-

¹GeoForschungsZentrum-Potsdam, Potsdam, Germany.

²Lamont-Doherty Earth Observatory of Columbia University, Palisades, New York, USA.

³Fachbereich Geowissenschaften, Universität Bremen, Bremen, Germany.

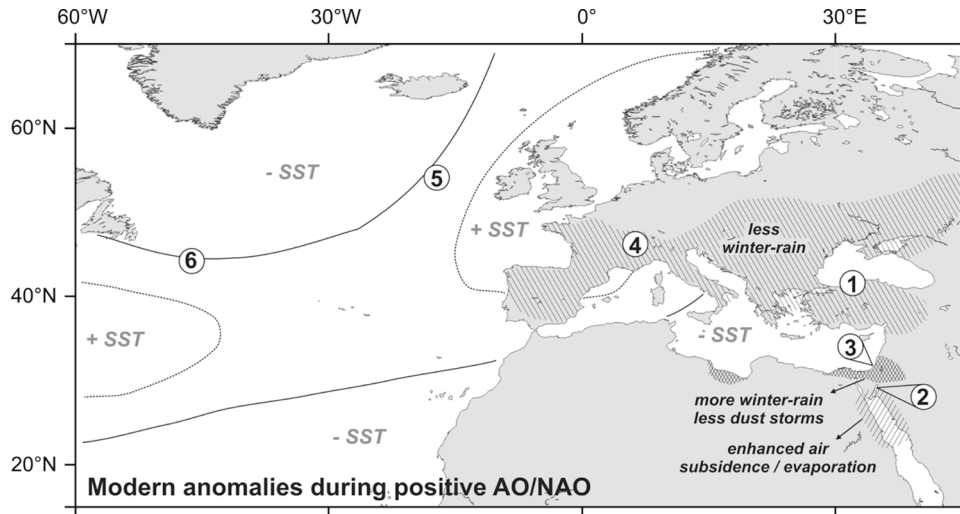


Figure 1. Map showing location of sites discussed in the text and the modern regional impact of positive AO/NAO anomalies (North Atlantic [Visbeck et al., 2003], Turkey [Cullen and deMenocal, 2000; Turkes and Erlat, 2003], and northern Red Sea/southern Israel [Cullen and deMenocal, 2000; Eshel et al., 2000; Rimbu et al., 2001; Zangvil et al., 2003]). Circled numbers indicate the following: 1, cores GeoB 7622-2 and GeoB 7625-2 (this study); 2, core GeoB 5804-4 (this study); 3, cores GA-112/GA-110 off southern Israel [Schilman et al., 2001]; 4, lake level reconstructions from the French/Swiss Jura Mountains [Magny, 2004]; and 5 and 6, North Atlantic sediment cores used for stacked drift ice record [Bond et al., 2001].

graphically elevated ridges on the continental slope away from the pathways of turbidity currents (Figure 2) and are thus particularly suitable for reconstructing past variations in the terrigenous input from rivers. The Sakarya River is the longest Anatolian river and drains parts of the central

Anatolian plain and the Pontide Mountains along the Black Sea [Algan et al., 1999] where interannual to decadal-scale rainfall changes in this Mediterranean-type winter rain climate region are strongly coupled to AO/NAO [Turkes and Erlat, 2003].

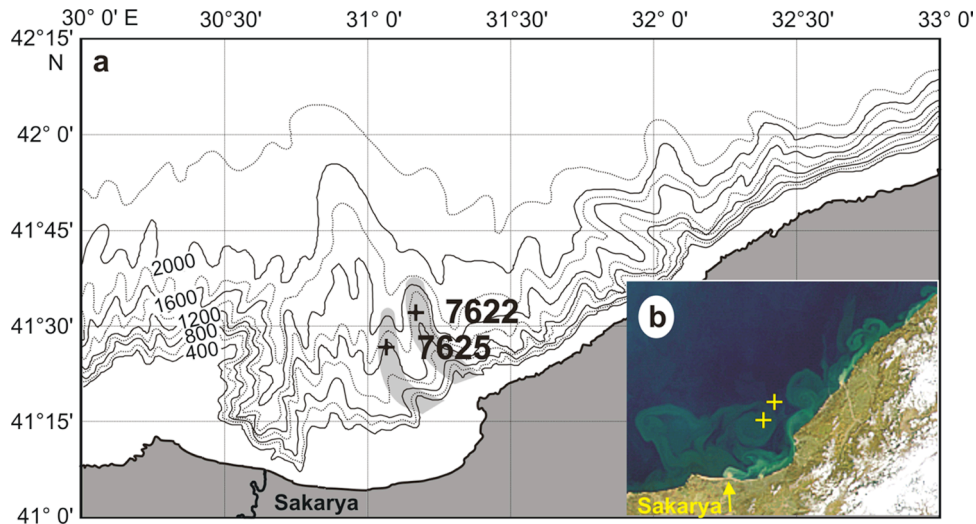


Figure 2. Regional setting of the Black Sea. (a) Detailed bathymetric map of the study area showing the location of cores GeoB 7622-2 and 7625-2 collected during R/V Meteor cruise 51-4 [Jørgensen and Cruise Participants, 2003]. Both sites are located on topographic ridges (gray shading) and should therefore not be influenced by resedimentation processes such as turbidity currents. A further argument for the fluvial origin of the clay layers is the observation of very similar clay layer frequency records at both sites (Figure 4) that are located on different topographic ridges. (b) Satellite image of the Sakarya River mouth with location of the sediment cores showing that both sites receive large amounts of suspended sediment originating from the river (source: <http://visibleearth.nasa.gov/>).

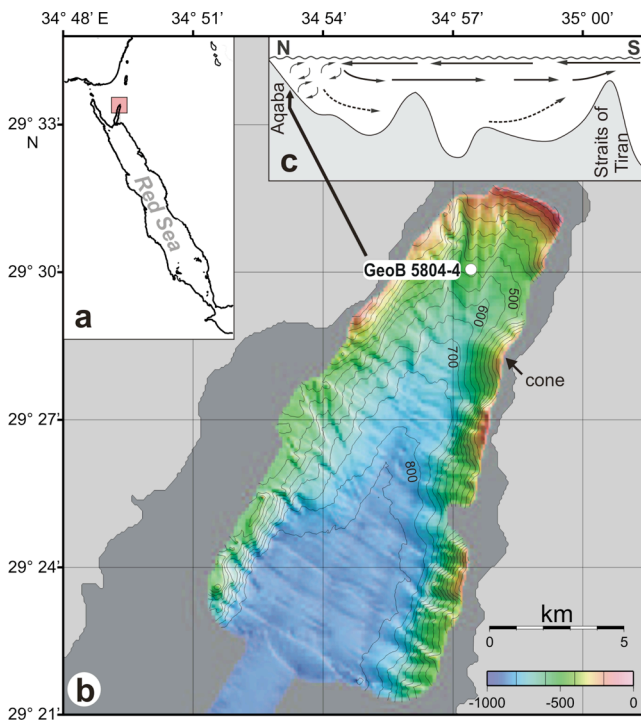


Figure 3. Regional setting of the Gulf of Aqaba. (a) Location of the northern Gulf of Aqaba as the northeastern extension of the Red Sea. (b) Detailed bathymetric map of the study area [after Ehrhardt *et al.*, 2005] showing the location of core GeoB 5804-4 collected during R/V *Meteor* cruise 44-3 [Pätzold and Cruise Participants, 1999]. (c) Schematic illustration of the predominantly thermohaline-driven circulation within the Gulf of Aqaba [after Eshel and Naik, 1997].

[5] Late glacial to Holocene sediments of the Black Sea are classically subdivided into three lithological units [Ross and Degens, 1974; Hay *et al.*, 1991]. The most recent one is unit I which is characterized by finely laminated coccolith ooze of late Holocene age. Unit II basically covers the middle Holocene and consists of likewise finely laminated sapropelic sediments. Both units were deposited under marine conditions (anoxic in the basin). Unit III sediments are lacustrine clays with occasional centimeter-scale laminations representing the glacial to early Holocene freshwater lake stage of the Black Sea. A recent view of the general late glacial to Holocene history of the Black Sea is given by Bahr *et al.* [2005] and Ryan *et al.* [2003].

2.2. Northern Red Sea

[6] Our study here is based on sediment core GeoB 5804-4 (29°30.1'N, 34°57.4'E; 464 m water depth) retrieved from the northernmost Gulf of Aqaba (Figure 3a). The coring site is located on an elevated ridge separated by two north-south oriented channel structures [Ehrhardt *et al.*, 2005], and should therefore not be influenced by resedimentation processes such as turbidity currents. Sediments are oxic and predominately siliciclastic with biogenic carbonate contents ranging around 30 wt % and low organic carbon contents (approximately 0.35 wt % on average). Sediments

delivered from the Wadi Mubarak (marked as cone in Figure 3b) are mainly displaced toward the southward extending Elat Deep (>800 m water depth) and sediment cores from this area show frequent intercalations of distinct sandy turbidites [Pätzold and Cruise Participants, 1999].

[7] The Gulf of Aqaba is located at the extreme north of the northern Red Sea thermohaline overturning cell [Eshel and Naik, 1997] where water mass stratification and deep water formation are particularly sensitive to temperature and aridity changes [Eshel *et al.*, 2000]. Figure 3c shows a schematic illustration of the predominantly thermohaline-driven circulation within the Gulf of Aqaba. Owing to an upper warm layer inflow from the Red Sea over a shallow sill (Straits of Tiran), the overall vertical stratification in the Gulf is unusually weak resulting in relatively warm, homogenous deep waters, which are formed in the northernmost Gulf of Aqaba during the cold winter months. Small interannual anomalies in surface water temperatures and densities result in episodic extreme deep convective mixing events (>850 m water depth) [Felis *et al.*, 1998; Genin *et al.*, 1995]. Presently, evaporation (~200 cm/yr) exceeds precipitation that is restricted to rare winter rain (10 to 25 mm/yr) originating from the southeastern Mediterranean Sea.

[8] Coral records that cover the past 250 years suggest a strong AO/NAO control on temperature and aridity variability on interannual and interdecadal timescales in the northern Red Sea region [Eshel *et al.*, 2000; Rimbu *et al.*, 2001]. Studies on fossil corals show that this high sensitivity to AO/NAO appears to be characteristic for both the late Holocene and the Eemian interglacial [Felis *et al.*, 2004].

3. Methods

3.1. Stratigraphy

[9] Age models for the Black Sea cores GeoB 7622-2 and GeoB 7625-2 were obtained by ^{14}C accelerator mass spectrometry (AMS) dating and recognition of a distinctive ash layer (Tables 1a and 1b). The two classical Black Sea units I and II [Ross and Degens, 1974; Hay *et al.*, 1991] can be clearly distinguished, e.g., on the basis of gray scale data (Figure 4a, see also section 4.1). However, compared to the classical Black Sea sequences, both cores reveal unusual high sedimentation rates due to the nearshore position close to the mouth of the Sakarya River resulting in enhanced terrigenous sediment input and the intercalation of homogenous clay layers (see section 4.1 for further details).

[10] Sediments of units I and II are generally laminated. On the basis of sediment trap studies [Hay *et al.*, 1990] and sedimentological analyses of laminated sequences from the Black Sea abyssal plains [Hay *et al.*, 1991], the laminae most likely represent annual varves. However, the trap studies suggest that the coccolithophoride blooms do not occur every year and a recent sedimentological study suggests that individual laminae may additionally be post-depositionally destroyed by large fecal pellets that form after exceptional productivity events [Pilskaln and Pike, 2001].

[11] Thus a more detailed age model for the Holocene Black Sea sediments must primarily rely on ^{14}C dating that

Table 1a. Details on Age Control Points Used to Construct the Age Model of of GeoB 7622-2 (7622-3), Black Sea

| Core Depth, cm | Laboratory Identification/Remarks | ¹⁴ C AMS Age, Years B.P. | ±Error, Years | Calibrated Age, Calendar Years B.P. |
|-----------------|-----------------------------------|-------------------------------------|---------------|-------------------------------------|
| MUC surface | surface of multicorer GeoB 7622-3 | | | modern age |
| 57 (54–60) | KIA 25671 ^a | 1170 | ±35 | 655 |
| 137 (134–140) | KIA 25749 ^a | 2095 | ±30 | 1580 |
| 233.5 (230–237) | KIA 25672 ^a | 2385 | ±35 | 1920 |
| 323 (320–326) | KIA 25751 ^a | 3080 | ±35 | 2760 |
| 400.0 | Santorini ash | | | 3595 ^b |
| 478 (476–480) | KIA 25674 ^a | 4605 | ±55 | 4785 |
| 520 | KIA 19273 ^c | 5715 | ±25 | 5430 ^d |
| 555 (553–557) | KIA 25675 ^a | 6590 | ±70 | 7005 |
| 564.5 (563–566) | KIA 25753 ^a | 7625 | ±55 | 7995 |

^aMonospecific carbonate samples of juvenile bivalve shells (*Mytilus galloprovincialis*).

^bAge after Hammer *et al.* [1987].

^cOrganic matter.

^dCorrected and calibrated after Jones and Gagnon [1994].

has however historically been hampered by the lack of suitable carbonate material for ¹⁴C dating. As a result, ¹⁴C dating of the Black Sea sequence in the basin has in the past been based almost entirely on bulk carbonate and organic carbon [e.g., Jones and Gagnon, 1994], both of which are very sensitive to terrestrial contamination. Careful analyses of our cores from the Turkish continental margin have revealed the presence of datable carbonate shells that are free of contamination problems. In most parts of the record, we found small (approximately 200 μm) and very well preserved shells that represent the larval stage of the mollusc *Mytilus galloprovincialis*. During this juvenile stage, *Mytilus galloprovincialis* is planktonic and therefore represents the age of the surface waters. We find the shells in comparatively high concentrations (we picked approximately 2000 individual shells per dating sample) because of the nearshore location of our sediment cores (Figure 2) where the *Mytilus* larvae are more abundant [Aral, 1999]. Therefore they could not be dated in previous studies that concentrated on the deep basin sediments.

[12] We further recognized an ash layer that has been previously found in sediments of the Black Sea and originates from the Minoan eruption of Santorini [Guichard *et al.*, 1993]. These age control points are complemented by an additional ¹⁴C AMS date on organic matter (core GeoB 7622-2) that we obtained from the older part of unit II. This sample was taken from the richest organic carbon interval that should be influenced by continental detrital carbon

input in a similar way as the basin sediments. We therefore performed the detrital carbon correction applied to the basin sediments [Jones and Gagnon, 1994]. Additional ¹⁴C ages obtained on core GeoB 7622-2 were substantially too old because of enhanced terrestrial carbon input to the continental slope in comparison to the basin. The ¹⁴C ages were corrected with a regional deviation from the global reservoir effect (ΔR) of ~70 years (according to the Marine Reservoir Correction Database, available at <http://depts.washington.edu/qil/marine/>) and converted to calendar years with the Calib 4.3 software (<http://depts.washington.edu/qil/>). We applied modern reservoir ages because the age of Black Sea surface waters should be largely controlled by the inflow of Mediterranean surface waters that do not show significant reservoir age changes during the Holocene [Siani *et al.*, 2001]. Considering the extraordinarily stable vertical stratification of the Black Sea, we assume that mixing with potentially older deep waters should not significantly affect the reservoir ages.

[13] Between individual dated levels we used a linear interpolation. All ages were measured on core GeoB 7622 and could be exactly transferred to core GeoB 7625 by careful visual inspection of the lamination pattern. Finally, we assumed a modern age for the surface of multicore GeoB 7622-3 that could be appended to the top of the two sediment cores, indicating that 20 cm and 33.5 cm of sediment are missing in core GeoB 7622-2 and GeoB 7625-2, respectively.

Table 1b. Details on Age Control Points Used to Construct the Age Model of GeoB 7625-2, Black Sea

| Core Depth, cm | Remarks | Calibrated Age, cal. Years B.P. |
|----------------|----------------------------------------------------------------------|---------------------------------|
| 0 | age assigned from correlation with GeoB 7622-2, 13.5 cm | 247 |
| 46 | age from correlation with GeoB 7622 ¹⁴ C date at 57 cm | 655 |
| 158 | age from correlation with GeoB 7622 ¹⁴ C date at 137 cm | 1580 |
| 293 | age from correlation with GeoB 7622 ¹⁴ C date at 233.5 cm | 1920 |
| 388 | age from correlation with GeoB 7622 ¹⁴ C date at 323 cm | 2760 |
| 466.2 | Santorini ash | 3595 ^a |
| 537.5 | age from correlation with GeoB 7622 ¹⁴ C date at 478 cm | 4785 |
| 578 | age from correlation with GeoB 7622 ¹⁴ C date at 520 cm | 5430 |
| 614 | age from correlation with GeoB 7622 ¹⁴ C date at 555 cm | 7005 |
| 624 | age from correlation with GeoB 7622 ¹⁴ C date at 564.5 cm | 7995 |

^aAge after Hammer *et al.* [1987].

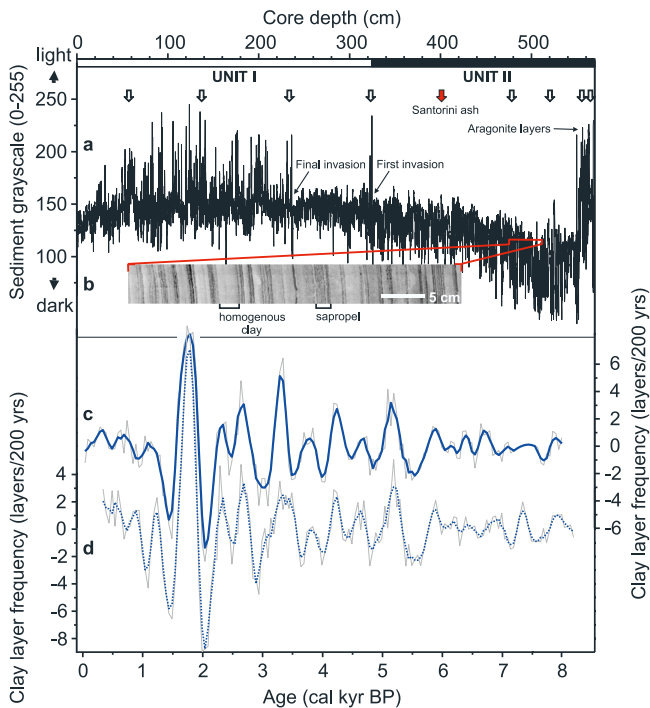


Figure 4. Black Sea records. (a) Gray scale record from core GeoB 7622-2 for visualization of Black Sea unit division [after Hay *et al.*, 1991] and indication of marker horizons. Arrows indicate ^{14}C AMS datings (Table 1a). (b) Detail of unit II sediments in core GeoB 7622-2 showing the intercalation of homogenous clay layers with finely laminated sapropelitic intervals. (c) Clay layer frequency record from core GeoB 7622-2 (and multicorer core GeoB 7622-2) showing pronounced multicentennial-scale variability (detrended data, thick line is three-point moving average). (d) Clay layer frequency record from core GeoB 7625-2 displays a very similar pattern ($r=0.83$) (detrended data, thick line is three-point moving average).

[14] The age model for Gulf of Aqaba core GeoB 5804-4 is based on eight ^{14}C AMS dates, conversion to calendar years with the Calib 4.3 software, and linear interpolation between these dates (Table 1c). We considered a regional deviation from the global reservoir effect (ΔR) of ~ 180 years based on recent dating of living corals in the northern Red Sea [Felis *et al.*, 2004]. With a sampling interval of 1 cm (for

oxygen isotopes below 250 cm core depth 2 cm), the average time resolution of the presented records is between 20 and 30 years.

3.2. Clay Layer Frequencies

[15] As further discussed in section 4.1, the records from the southwestern Black Sea are characterized by frequent intercalation of homogenous clay layers (Figure 4b). Visual counting of these clay layers was performed on split sediment cores and X-ray radiographs by counting every clay layer greater than 0.3 cm in thickness resulting in ~ 270 and ~ 310 layers in core GeoB 7622-2 and GeoB 7625-2, respectively, implying a recurrence time of ~ 25 years. The record was extended to the present by appending the clay layers in multicorer core GeoB 7622-3. Clay layer frequencies were calculated for 200-year time windows shifted in 50-year steps along the record. The resulting frequency curve was detrended by subtracting a 1000-year moving average.

3.3. Stable Oxygen Isotopes

[16] Stable oxygen isotope measurements on core GeoB 5804-4 have been performed on shells of the planktic foraminifer *Globigerinoides ruber* (white) and the benthic foraminifer *Cibicides mabahethi* employing an automatic carbonate preparation system (Kiel device) attached to a Finnigan MAT 251 mass spectrometer. To avoid size-dependent effects on the $\delta^{18}\text{O}$ values and to reduce potential intrasample noise, 50 specimens of 350- to 400- μm diameter (measured along the longest axis) *G. ruber* (white) were hand-picked and homogenized before measurement. The ratio of $^{18}\text{O}/^{16}\text{O}$ is given in ‰ relative to the VPDB standard. Analytical standard deviation is about $\pm 0.07\%$ PDB (Isotope Lab, Bremen University).

3.4. Sand Accumulation Rates

[17] Sand accumulation rates were calculated from terrigenous sand contents ($>63\ \mu\text{m}$) data that were obtained by wet sieving of the carbonate and organic-matter-free sediment samples of core GeoB 5804-4. The major part ($\sim 80\%$) of the sand fraction is $<150\ \mu\text{m}$ (fine to very fine sand).

3.5. Spectral Analyses

[18] Spectral analyses were performed with the AnalySeries software package [Paillard *et al.*, 1996]. Spectra were calculated following the classical and very robust Blackman-Tukey method. The algorithm computes first the autocovariance of the data, applies a Tukey window, and

Table 1c. Details on Age Control Points Used to Construct the Age Model of GeoB 5804-4, Gulf of Aqaba, Northern Red Sea

| Laboratory Identification | Core Depth, cm | Foraminifera Species | ^{14}C AMS Age, Years B.P. | \pm Error, Years | Calibrated Age, Calendar Years B.P. |
|---------------------------|----------------|-------------------------|-------------------------------------|--------------------|-------------------------------------|
| KIA8615 | 0 | <i>G. sacculifer</i> | 440 | 25 | after A.D. 1950 |
| KIA8614 | 50 | <i>G. sacculifer</i> | 1900 | 25 | 1272 |
| KIA8613 | 100 | <i>G. ruber</i> (white) | 2700 | 35 | 2158 |
| KIA8611 | 150 | <i>G. sacculifer</i> | 4110 | 50 | 3897 |
| KIA8610 | 200 | <i>G. sacculifer</i> | 5095 | 35 | 5270 |
| KIA8609 | 250 | <i>G. sacculifer</i> | 6210 | 40 | 6435 |
| KIA8607 | 300 | <i>G. sacculifer</i> | 6595 | 45 | 6882 |
| KIA8606 | 329 | <i>G. sacculifer</i> | 6940 | 60 | 7274 |

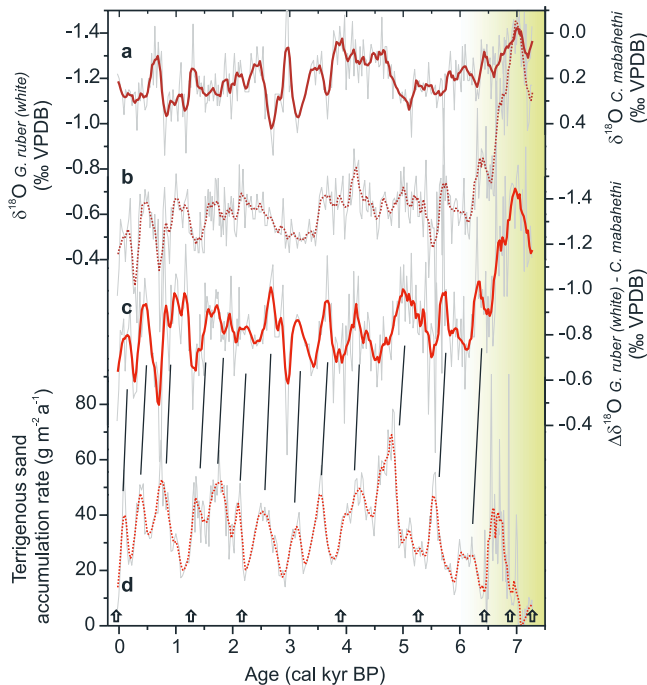


Figure 5. Original (undetrended) paleoenvironmental data from the northern Red Sea (core GeoB 5804-1). (a) Stable oxygen isotope ($\delta^{18}\text{O}$) record of the epibenthic foraminifera *Cibicoides mabahethi* (thick line is five-point moving average). (b) The $\delta^{18}\text{O}$ record of the planktic foraminifera (*Globigerinoides ruber* (white) (dotted line is five-point moving average). (c) Stable oxygen isotope difference ($\Delta\delta^{18}\text{O}$) between planktic (*Globigerinoides ruber* (white)) and epibenthic foraminifera (*Cibicoides mabahethi*) as a proxy for changes in water column stratification (thick line is five-point moving average). (d) Terrigenous sand accumulation record (dotted line is five-point moving average). Black lines show systematic lag (maximum correlation between sand accumulation and isotopes at a lag of 125 years) of the multicentennial changes in the sand record compared to the very similar variations in $\Delta\delta^{18}\text{O}$. Arrows indicate ^{14}C datings (Table 1c). Shading marks the early Holocene humid period in the region [after Arz et al., 2003a].

finally Fourier transforms the covariance functions to compute the power spectrum. We applied a 50-year sampling interval, 73 lags, and 0.00041 bandwidth. Prior to spectral analyses, we removed potential millennial-scale variability by detrending the records in order to further enhance the dominant multicentennial-scale changes in the records.

4. Results and Discussion

4.1. Proxy Records From the Southwestern Black Sea and Northern Red Sea

[19] The analyzed sedimentary sequence from the southwestern Black Sea was deposited during the most recent anoxic phase of the Black Sea covering the marine Black Sea units I and II [Hay et al., 1991] and is laminated

throughout. The gray scale record shown in Figure 4a visualizes major characteristics of units I and II known from the abyssal sediments. Close to the base of the sapropel unit II, light colors reflect the occurrence of anorganically precipitated aragonite layers found throughout the Black Sea [e.g., Hay et al., 1991]. Within unit II, excursions toward low gray scale values reflect intervals with dominating sapropelic layers. The first invasion of the coccolithophoride *E. huxleyi* into the Black Sea marks the base of unit I, when the salinity of the Black Sea exceeded for the first time the tolerance level of this species [e.g., Hay et al., 1991], and is shown in the gray scale record by the occurrence of light laminae. The same applies for the final invasion of *E. huxleyi* after a short interval of reduced salinities [Hay et al., 1991].

[20] Regional sedimentation rates on the southwestern Black Sea continental slope are an order of magnitude higher than on the abyssal plains because of enhanced terrigenous sediment input. This enhanced sediment input is manifested in frequent intercalations of homogeneous clay layers that interrupt finely laminated intervals of predominating sapropelic sediments (unit II) and coccolith ooze (unit I) (Figure 4b). The homogenous clay layers most likely represent suspension fallout events from the Sakarya River plume related to increased winter rain in its western Anatolian drainage basin (see modern sediment plume in Figure 2b). In order to infer centennial-scale rainfall changes, we counted the homogenous clay layers that were visually distinguishable. Subtracting the counted clay layers from the sequence still leaves enhanced sedimentation rates at our sites suggesting that we do not cover the fluvial sediment input completely. The major record of multicentennial-scale changes should however be well captured by our layer counting.

[21] The resulting frequency records show distinct variations on multicentennial timescales that are very well correlated between the two cores (Figures 4c and 4d). The fact that the cores are located on different topographic ridges (Figure 2a) strengthens our assumption that we record regional fluvial sediment input originating from the Sakarya River and thus long-term Anatolian rainfall changes. Modern AO/NAO-related rainfall anomalies in this region are negative (positive) during phases of more positive (negative) AO/NAO [Turkes and Erlat, 2003], and would therefore be associated with intervals of lower (higher) clay layer frequencies.

[22] In order to reconstruct regional changes in hydroclimatic conditions in the northern Red Sea area, we use two different types of proxy data. Our primary data are stable oxygen isotope records based on epibenthic (*Cibicoides mabahethi*) and surface dwelling (*Globigerinoides ruber* (white)) foraminifera (Figures 5a and 5b). The difference between the stable oxygen isotope composition of the planktic ($\delta^{18}\text{O}_{\text{pl}}$) and epibenthic species records past changes in the vertical $\delta^{18}\text{O}$ gradient ($\Delta\delta^{18}\text{O}$) providing an indicator for the stratification of the water column in the northern Gulf of Aqaba (Figure 5c). The undetrended $\Delta\delta^{18}\text{O}$ record shows a major shift from ~ 7 to ~ 6.25 kyr B.P. that relates to the end of the early Holocene humid period in the region [Arz et al., 2003a]. During this period, freshwater

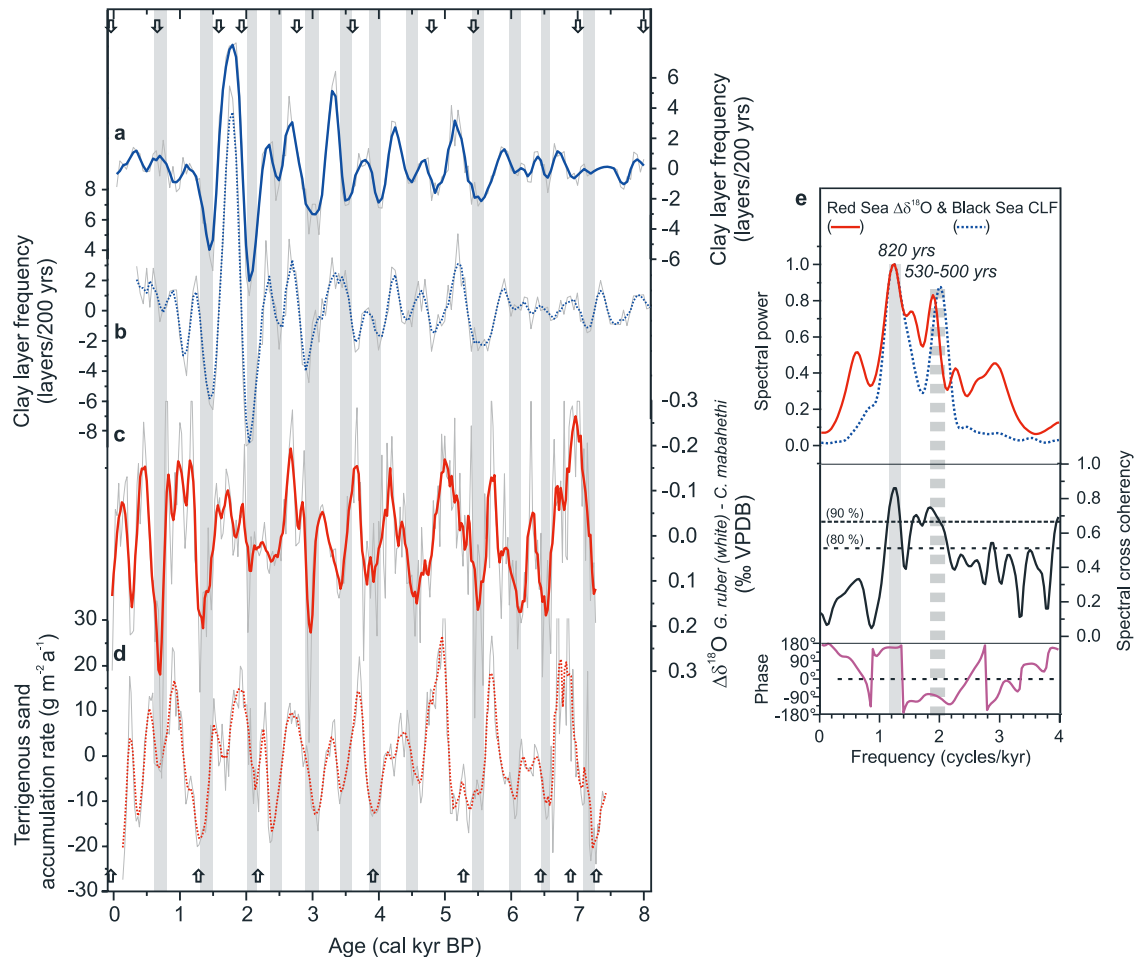


Figure 6. Proxy records from the southwestern Black Sea and the northernmost Red Sea. (a) Clay layer frequency record from core GeoB 7622-2 as shown in Figure 4. Arrows indicate ^{14}C AMS datings. (b) Clay layer frequency record from core GeoB 7625-2 as shown in Figure 4. (c) Stable oxygen isotope difference ($\Delta\delta^{18}\text{O}$) between planktic (*Globigerinoides ruber* (white)) and epibenthic foraminifera (*Cibicidoides mabahethi*) as a proxy for changes in water column stratification (core GeoB 5804-4, detrended data, original data shown in Figure 5, thick line is five-point moving average). (d) Terrigenous sand accumulation rate as a proxy for dust input to the northern Gulf of Aqaba (core GeoB 5804-4, detrended data set shifted by 125 years, original data shown in Figure 4, dotted line is five-point moving average). Arrows indicate ^{14}C AMS datings. Gray bars indicate proposed graphic correlation between the records. (e) Spectral analyses. Clay layer frequency (CLF) record (GeoB 7622, red line) and Red Sea $\Delta\delta^{18}\text{O}$ record (blue line) with cross spectral coherence between both records at the 80% and 90% confidence levels and phasing is shown. Labels indicate major coherent periods in the data sets. The $\sim 180^\circ$ phasing of the ~ 800 -year cycle suggests hydroclimatic changes in both regions similar to those presently observed during AO/NAO extremes.

input substantially decreased salinity and thus the $\delta^{18}\text{O}$ of surface waters in the northern Red Sea [Arz *et al.*, 2003a]. Besides this large long-term shift, a number of smaller-scale variations suggest substantial multicentennial-scale perturbations (Figure 6c). At the latest with the end of the humid period at ~ 6.25 kyr B.P., the direct effect of freshwater input on $\delta^{18}\text{O}$ becomes negligible and it is reasonable to assume that, since then, $\delta^{18}\text{O}$ variations are primarily a response to changes in temperature and evaporation.

[23] A coral-based $\delta^{18}\text{O}$ record from the northern Red Sea [Eshel *et al.*, 2000] has been used as a direct proxy for surface water density changes and related deep water mass

formation during the past decades. That study suggests that northern Red Sea deep water formation is strongly coupled to large-scale atmospheric processes in the eastern Mediterranean region involving a subsiding air flow from the eastern Mediterranean toward the northern Red Sea region. These large-scale atmospheric processes appear to be closely coupled to AO/NAO. During positive AO/NAO, an anomalously high pressure system covers large parts of the Mediterranean resulting in northerly winds in the eastern part that drive the advection of dry and cold air. This enhances the surface water densities in the northern Red Sea and weakens the water column stratification [Eshel and Farrell, 2000;

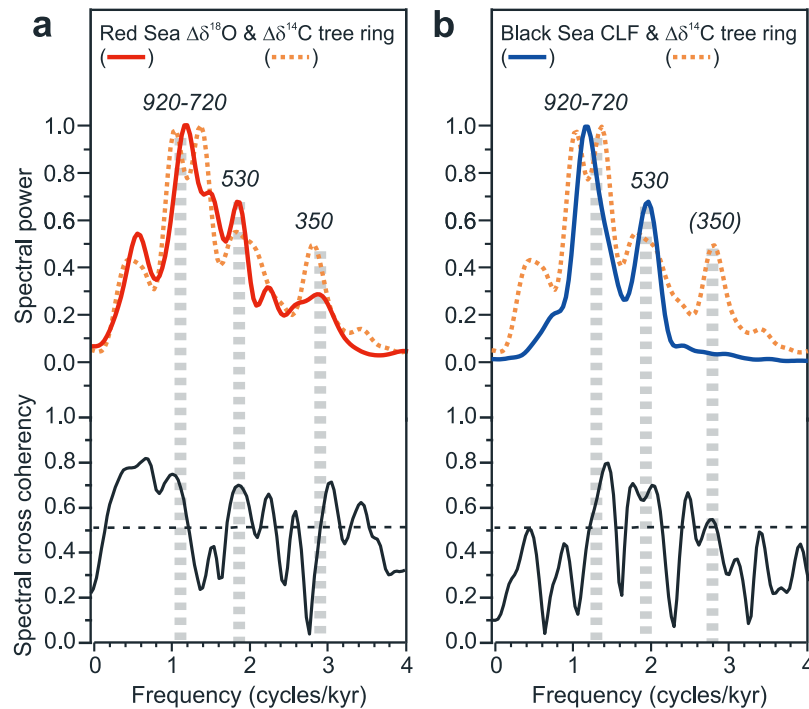


Figure 7. Comparison of (a) Red Sea $\Delta\delta^{18}\text{O}$ record and (b) Black Sea clay layer frequency (CLF) to the tree ring-based residual $\Delta^{14}\text{C}$ record as a proxy for solar variability [Stuiver *et al.*, 1998] to show similar multicentennial-scale variability. Blackman-Tukey spectra of the detrended records as shown in Figure 6 and cross spectral coherency at the 80% confidence level are depicted. Labels indicate major coherent periods in the data sets.

Eshel *et al.*, 2000; Felis *et al.*, 2000; Rimbu *et al.*, 2001]. We assume that direct impacts of changes in the tropical monsoon system can only be minor because of the predominating control of extratropical atmospheric circulation changes on the northern Red Sea over a wide range of timescales during the Holocene [Arz *et al.*, 2003a; Felis *et al.*, 2004], last glacial [Arz *et al.*, 2003b], and previous interglacial [Felis *et al.*, 2004].

[24] Our second, independent data set from the Red Sea is the terrigenous sand accumulation record as an indicator of changes in the eolian input from the surrounding desert areas (Figure 5d). After removing the long-term trend, which is mainly related to the transition from the Holocene humid period to the present arid conditions (Figure 5d), the high-resolution record shows repeated periods of reduced and enhanced sand accumulation reoccurring on multicentennial timescales (Figure 6d) that are remarkably similar to the changes in water stratification recorded in our $\Delta\delta^{18}\text{O}$ record (Figure 6c). However, the multicentennial changes in the sand record appear to systematically lag the very similar variations in $\Delta\delta^{18}\text{O}$ (maximum correlation between sand accumulation and isotopes at a lag of 125 years; Figure 5d). It is unlikely that eolian sediment input and water column stratification show a different response time as both processes are controlled by atmospheric processes. Therefore the lag is most likely induced by differential mixing processes through bioturbation as observed in several studies [e.g., Brown *et al.*, 2001]. Such processes generally produce younger apparent ages for finer-grained material (in

our case the predominantly fine to very fine-grained sand; $<150\ \mu\text{m}$) than for coarser-grained particles (in our case foraminifera; 350 to 400 μm).

[25] Lower sand accumulation occurred during periods of weaker water column stratification, which today are associated with intervals of more positive AO/NAO. A potential mechanism would be reduced aridity during such periods. Regional rainfall in southernmost Israel (close to the Gulf of Aqaba) indeed tends to increase during positive AO/NAO intervals as for example during the period 1975–1995 [Zangvil *et al.*, 2003]. Likewise on longer timescales, surface water reconstructions on planktic foraminifera off southern Israel [Schilman *et al.*, 2001] (Figure 1) covering the last circa 3500 years, suggest repeated intervals of more humid (and/or warmer) conditions that roughly correlate to our intervals of lower sand accumulation and weaker water column stratification. However, considering the hyperarid conditions of the region, aridity changes cannot be the only reason for changes in eolian supply. Also conceivable is a relation to the frequency and intensity of dust storms. The majority of dust storms in Israel are associated with south-westerly winds during intervals of strong low-pressure systems in the eastern Mediterranean (Cyprus Low) [Pye, 1987] as presently occurring during negative AO/NAO phases [Hurrell, 1995; Zangvil *et al.*, 2003].

4.2. Long-Term Changes in AO/NAO?

[26] Taken together, our independent proxy records from the Black Sea and Red Sea show similar multicentennial

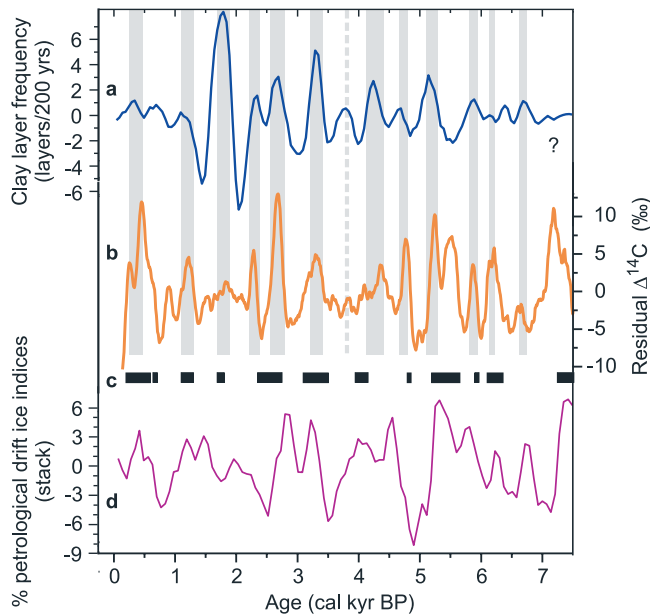


Figure 8. Comparison of the Black Sea record to the solar variability and other relevant records. (a) Clay layer frequency record in southwestern Black Sea (core GeoB 7622 as shown in Figure 6). More (less) frequent clay layers are interpreted to represent negative (positive) AO/NAO phases. (b) Residual $\Delta^{14}\text{C}$ record as a proxy for solar variability (positive $\Delta^{14}\text{C}$ representing reduced solar output, detrended decadal data set smoothed with a 13-point moving average) [Stuiver *et al.*, 1998]. (c) Lake level highstands in the French/Swiss Jura Mountains interpreted to represent a southward displacement of the Atlantic westerly jet [Magny, 2004] as presently occurring during negative AO/NAO phases. (d) Stacked drift ice record from the North Atlantic [Bond *et al.*, 2001]. Less (more) drift ice represents warmer (cooler) sea surface temperatures (negative AO/NAO, see text for discussion).

variability over the past ~ 7500 years (Figure 6). Spectral analyses of the Black Sea clay layer frequencies and the Red Sea $\Delta\delta^{18}\text{O}$ record show prominent multicentennial cycles at ~ 800 and ~ 500 years, both of which reveal significant cross coherence (Figure 6e). The phasing of the dominant cycle at ~ 800 years is clearly antiphased in both records ($\sim 180^\circ$), whereas the ~ 500 -year cycle reveals a phasing of $\sim 100^\circ$. The deviation from a strict antiphasing is probably induced by dating limitations due to small errors in ^{14}C dating, reservoir age corrections, and interpolation between the dating points. The latter likewise applies to the graphic correlation between the records that shows a general antiphased pattern but reveals some remaining ambiguities (Figures 6a–6d). In addition, the multicentennial changes in our Black Sea and Red Sea records show a different amplitude evolution. While the amplitudes in the Red Sea records (Figures 6c and 6d) do not vary significantly, there are large fluctuations in the amplitudes of the clay layer frequency records from the

Black Sea (Figures 6a and 6b), particularly the low amplitudes in the early part of the record and the large swing between circa 1.5 and 2 kyr B.P. The low amplitudes are likely related to substantially decreased sedimentation rates that decrease the resolution of the record and deteriorate the visual distinction of individual clay layers. The low sedimentation rates could be the expression of dryer conditions during the early part of the record that would correspond to the early Holocene humid period in the Red Sea [Arz *et al.*, 2003a] and may suggest an “antiphasing” likewise on longer than multicentennial timescales [Rimbu *et al.*, 2003]. The large-amplitude change in the late Holocene probably reflects a very humid interval in Anatolia. The Red Sea records shown in this paper do not show a particular event during this interval but preliminary planktic foraminifera census counts in the whole northern Red Sea suggest anomalous surface water conditions during this interval.

[27] The antiphasing between the records shown in both the spectral analyses results and the graphic correlation (Figure 6) suggests a multicentennial pattern similar to modern AO/NAO–related environmental changes on inter-annual to interdecadal timescales in both regions: Intervals of reduced (enhanced) clay layer frequency and thus less (more) Anatolian rainfall recorded in our Black Sea cores (Figures 6a and 6b) were accompanied by increased (decreased) surface water densities, substantially reduced (enhanced) water stratification (Figure 6c), and less (more) intense dust transport in the northern Red Sea region (Figure 6d) implying more frequent or more persistent positive (negative) AO/NAO conditions (Figure 1).

[28] Holocene climate fluctuations on different timescales have been linked to decadal- to multicentennial-scale variations in solar activity [Bond *et al.*, 2001; Fleitmann *et al.*, 2003]. Comparing our records to the tree ring based residual $\Delta^{14}\text{C}$ record as a proxy for solar variability [Stuiver *et al.*, 1998] shows that similar multicentennial cycles are present in the records. Spectral analyses of the $\Delta^{14}\text{C}$ record reveal dominant peaks at $\sim 720/920$, ~ 530 , and ~ 350 years that are close to the ~ 800 - and ~ 500 -year cycles found in our Black Sea and Red Sea records (Figure 7) (a cycle of ~ 350 years appears to be present only in the Red Sea $\Delta\delta^{18}\text{O}$ record). The graphic correlation suggests that intervals of more negative AO/NAO (higher clay layer frequencies) relate, within dating uncertainties, to reduced solar activity (Figures 8a and 8b). This relationship is consistent with a modeling study on the AO/NAO pattern during the Maunder solar output minimum [Shindell *et al.*, 2001]. Further support comes from well-dated lake level records in the French/Swiss Jura Mountains (Figure 1) that were originally interpreted to represent latitudinal displacements of the Atlantic westerly jet linked to solar variability [Magny, 2004]. However, such displacements presently also occur in relation to AO/NAO [Hurrell, 1995] implying that higher lake levels (Figure 8c) may represent more negative AO/NAO phases. In addition, several studies from the Mediterranean Sea have described a number of cold spells reoccurring on millennial timescales during the Holocene [e.g., Cacho *et al.*, 2001; Rohling *et al.*, 2002; Sbaifi *et al.*, 2004]. Though the individual records are of lower time

resolution and thus mainly capture millennial-scale variability, we note that in particular the Aegean records of Rohling *et al.* [2002] could be interpreted in terms of atmospheric forcing involving AO/NAO as well (polar/continental air outbreaks and associated SST cooling in the Aegean Sea occur more frequently during positive AO/NAO [Rimbu *et al.*, 2003]).

[29] Our findings, on the other hand, appear to be in conflict with the previous conclusions derived from North Atlantic drift ice records [Bond *et al.*, 2001] (Figure 8d). At least during the late Holocene, increased drift ice associated with cooler surface water temperatures south of Greenland occurred during basin-wide cold phases recorded in Europe, Greenland, and the subtropical North Atlantic [Bond *et al.*, 2001], a pattern that is clearly distinct from the modern AO/NAO temperature anomalies in that region [Visbeck *et al.*, 2003] (Figure 1). However, it has been recently suggested that the North Atlantic temperature response to AO/NAO may be substantially different on multidecadal or longer timescales [Visbeck *et al.*, 2003]. Owing to a larger involvement of ocean circulation changes, including changes in the large-scale North Atlantic thermohaline circulation, a basin-wide temperature response to prolonged AO/NAO forcing is conceivable [Visbeck *et al.*, 2003] and would result in North Atlantic cooling during long-term negative AO/NAO intervals, a response consistent with the proxy records (Figure 8).

5. Conclusions

[30] Paleoenvironmental proxy data for hydroclimatic changes in northern Anatolia and the northern Red Sea region show multicentennial-scale variations during the last

~7500 years that strongly resemble modern AO/NAO-related temperature and rainfall anomalies. Taken together, the available data suggest a prominent role of AO/NAO-like atmospheric variability during the Holocene beyond interannual to interdecadal timescales. The multicentennial variability appears to be similar to changes observed in proxy records for solar output changes.

[31] In remote, more continental regions, our records show large-scale atmospheric circulation changes and resulting hydroclimatic shifts with spatial patterns similar to the modern AO/NAO, most likely forced ultimately by solar output changes. In contrast, changes in the North Atlantic are distinct from the modern AO/NAO temperature anomalies in that region. The exact physical mechanism that transfers small solar irradiance changes either to symmetric responses in the North Atlantic circulation or to atmospheric circulation changes involving an AO/NAO-like pattern, remains unclear. Further research is needed to better understand the oceanic response and associated feedbacks of the Northern Hemisphere atmospheric circulation. Such findings are a major prerequisite to obtaining more reliable forecasts of the behavior of the AO/NAO on longer timescales, as particularly the impact of (natural) centennial-scale climate variability on future climate projections could be more substantial than previously thought [Moberg *et al.*, 2005].

[32] **Acknowledgments.** We thank M. Segl and B. Meyer-Schack, University of Bremen, for carrying out the stable isotope measurements. T. Felis and G. Haug contributed with helpful comments on earlier versions of the manuscript that, in addition, greatly benefited from the constructive reviews of P. deMenocal and G. Schmiedl. Financial support was made available through the Deutsche Forschungsgemeinschaft (LA 1273/2-1, LA 1273/2-2, and WE 992/47-3). F. Lamy and H. W. Arz contributed equally to the paper.

References

- Algan, O., C. Gazioglu, N. Cagatay, Z. Yücel, and B. Gönencgil (1999), Sediment and water influxes into the Black Sea by Anatolian rivers, *Z. Geomorphol.*, *43*, 61–79.
- Aral, O. (1999), Growth of the Mediterranean mussel (*Mytilus galloprovincialis* Lam., 1819) on Ropers in the Black Sea, Turkey, *Turk. J. Vet. Anim. Sci.*, *23*, 183–189.
- Arz, H. W., F. Lamy, J. Pätzold, P. J. Müller, and M. Prins (2003a), Mediterranean moisture source for an early-Holocene humid period in the northern Red Sea, *Science*, *300*, 118–122.
- Arz, H. W., J. Pätzold, P. J. Müller, and M. O. Moammer (2003b), Influence of Northern Hemisphere climate and global sea level rise on the restricted Red Sea marine environment during termination I, *Paleoceanography*, *18*(2), 1053, doi:10.1029/2002PA000864.
- Bahr, A., F. Lamy, H. Arz, H. Kuhlmann, and G. Wefer (2005), Late glacial to Holocene climate and sedimentation history in the NW Black Sea, *Mar. Geol.*, *214*, 309–322.
- Bond, G., B. Kromer, J. Beer, R. Muscheler, M. N. Evans, W. Showers, S. Hoffmann, R. Lottibond, I. Hajdas, and G. Bonani (2001), Persistent solar influence on north Atlantic climate during the Holocene, *Science*, *294*, 2130–2136.
- Brown, L., G. T. Cook, A. B. MacKenzie, and J. Thomson (2001), Radiocarbon age profiles and size dependency of mixing in northeast Atlantic sediments, *Radiocarbon*, *43*, 929–937.
- Cacho, I., J. O. Grimalt, M. Canals, L. Sbaffi, N.J. Shackleton, J. Schofield, and R. Zahn (2001), Variability of the western Mediterranean sea surface temperature during the last 25,000 years and its connection with the Northern Hemisphere climatic changes, *Paleoceanography*, *16*, 40–52.
- Cook, E. R., R. D. D'Arrigo, and M. E. Mann (2002), A well-verified, multiproxy reconstruction of the winter North Atlantic Oscillation index since A. D. 1400, *J. Clim.*, *15*, 1754–1764.
- Cullen, H. M., and P. B. deMenocal (2000), North Atlantic influence on Tigris-Euphrates streamflow, *Int. J. Clim.*, *20*, 853–863.
- Cullen, H. M., R. D. D'Arrigo, E. R. Cook, and M. E. Mann (2001), Multiproxy reconstructions of the North Atlantic oscillation, *Paleoceanography*, *16*, 27–39.
- Ehrhardt, A., C. Hübscher, Z. Ben-Avraham, and D. Gajewski (2005), Seismic study of pull-apart-induced sedimentation and deformation in the northern Gulf of Aqaba (Elat), *Tectonophysics*, *396*, 59–79.
- Eshel, G., and N. H. Naik (1997), Climatological coastal jet collision, intermediate water formation, and the general circulation of the Red Sea, *J. Phys. Oceanogr.*, *27*(7), 1233–1257.
- Eshel, G., and B. F. Farrell (2000), Mechanisms of eastern Mediterranean rainfall variability, *J. Atmos. Sci.*, *57*, 3219–3232.
- Eshel, G., D. P. Schrag, and B. F. Farrell (2000), Troposphere-planetary boundary layer interactions and the evolution of ocean surface density: Lessons from Red Sea corals, *J. Clim.*, *13*, 339–351.
- Felis, T., G. Lohmann, H. Kuhnert, S. J. Lorenz, D. Scholz, J. Pätzold, S. A. Al-Rousan, and S. M. Al-Moghrabi (2004), Increased seasonality in Middle East temperatures during the last interglacial period, *Nature*, *429*, 164–168.
- Felis, T., J. Pätzold, Y. Loya, M. Fine, A. H. Nawar, and G. Wefer (2000), A coral oxygen isotope record from the northern Red Sea documenting NAO, ENSO, and North Pacific teleconnections on Middle East climate variability since the year 1750, *Paleoceanography*, *15*, 679–694.
- Felis, T., J. Pätzold, Y. Loya, and G. Wefer (1998), Vertical water mass mixing and plankton blooms recorded in skeletal stable carbon isotopes of a Red Sea coral, *J. Geophys. Res.*, *103*, 30,731–30,740.

- Fleitmann, D., S. J. Burns, M. Mudelsee, U. Neff, J. Kramers, A. Mangini, and A. Matter (2003), Holocene forcing of the Indian monsoon recorded in a stalagmite from southern Oman, *Science*, *300*, 1737–1739.
- Genin, A., B. Lazar, and S. Brenner (1995), Vertical mixing and coral death in the Red Sea following the eruption of Mount Pinatubo, *Nature*, *377*, 507–510.
- Guichard, F., S. Carey, M. A. Arthur, H. Sigurdsson, and M. Arnold (1993), Tephra from the Minoan eruption of Santorini in sediments of the Black Sea, *Nature*, *363*, 610–612.
- Hammer, C. U., H. B. Clausen, W. L. Friedrich, and H. Tauber (1987), The Minoan eruption of Santorini in Greece dated to 1645 BC?, *Nature*, *328*, 517–519.
- Hay, B. J., M. A. Arthur, W. E. Dean, E. D. Neff, and S. Honjo (1991), Sediment deposition in the late Holocene abyssal Black Sea with climatic and chronological implications, *Deep Sea Res. Part A*, *38*, suppl. 2, S1211–S1235.
- Hay, B. J., S. Honjo, S. Kempe, V. A. Ittekkot, E. T. Degens, T. Konuk, and E. Izdar (1990), Interannual variability in particle flux in the southwestern Black Sea, *Deep Sea Res., Part A*, *37*, 911–928.
- Hurrell, J. W. (1995), Decadal trends in the North Atlantic oscillation: Regional temperatures and precipitation, *Science*, *269*, 676–679.
- Jones, G. A., and A. R. Gagnon (1994), Radiocarbon chronology of Black Sea sediments, *Deep Sea Res., Part I*, *41*, 531–557.
- Jørgensen, B. B. and Cruise Participants (2003), METEOR-Berichte, Cruise 51, Leg 4, Istanbul–Istanbul, *METEOR-Ber. 03-1*, 57 pp., Cent. for Mar. Environ. Sci., Bremen, Germany.
- Keigwin, L. D., and R. S. Pickart (1999), Slope water current over the Laurentian Fan on interannual to millennial time scales, *Science*, *286*, 520–523.
- Luterbacher, J., et al. (2001), Extending North Atlantic oscillation reconstructions back to 1500, *Atmos. Sci. Lett.*, *2*, 114–124.
- Magny, M. (2004), Holocene climate variability as reflected by mid-European lake-level fluctuations and its probable impact on prehistoric human settlements, *Quat. Int.*, *113*, 65–79.
- Moberg, A., D. M. Sonechkin, K. Holmgren, N. M. Datsenko, and W. Karlen (2005), Highly variable Northern Hemisphere temperatures reconstructed from low- and high-resolution proxy data, *Nature*, *433*, 613–617.
- Noren, A. J., P. R. Bierman, E. J. Steig, A. Lini, and J. Southon (2002), Millennial-scale storminess variability in the northeastern United States during the Holocene epoch, *Nature*, *419*, 821–824.
- Paillard, D., L. Labeyrie, and P. Yiou (1996), Macintosh program performs time-series analysis, *Eos Trans. AGU*, *77*(39), 379.
- Pätzold, J. and Cruise Participants (1999), Report and preliminary results of Meteor Cruise M 44/3, Aqaba (Jordan)–Safaga (Egypt)–Dubai (Saudi Arabia)–Suez (Egypt)–Haifa (Israel), March 12–March 26–April 2–April 4, 1999, *Rep. 149*, 135 pp., Dep. of Geosci., Univ. Bremen, Bremen, Germany.
- Pilskaln, C. H., and J. Pike (2001), Formation of Holocene sedimentary laminae in the Black Sea and the role of the benthic flocculent layer, *Paleoceanography*, *16*, 1–19.
- Pye, K. (1987), *Aeolian Dust and Dust Deposits*, 334 pp., Elsevier, New York.
- Rimbu, N., G. Lohmann, T. Felis, and J. Pätzold (2001), Arctic oscillation signature in a Red Sea coral, *Geophys. Res. Lett.*, *28*, 2959–2962.
- Rimbu, N., G. Lohmann, J. H. Kim, H. W. Arz, and R. Schneider (2003), Arctic/North Atlantic Oscillation signature in Holocene sea surface temperature trends as obtained from alkenone data, *Geophys. Res. Lett.*, *30*(6), 1280, doi:10.1029/2002GL016570.
- Rohling, E. J., P. A. Mayewski, R. H. Abu Zied, J. S. L. Casford, and A. Hayes (2002), Holocene atmosphere-ocean interactions: Records from Greenland and the Aegean Sea, *Clim. Dyn.*, *18*, 587–594.
- Ross, D., and E. T. Degens (1974), Recent sediments of Black Sea, in *The Black Sea—Geology, Chemistry and Biology*, edited by E. T. Degens and D. Ross, pp. 183–199, Am. Assoc. of Pet. Geol., Tulsa, Okla.
- Ryan, W. B. F., C. O. Major, G. Lericolais, and S. L. Goldstein (2003), Catastrophic flooding of the Black Sea, *Annu. Rev. Earth Planet. Sci.*, *31*, 525–554.
- Sbaffi, L., F. C. Wezel, G. Curzi, and U. Zoppi (2004), Millennial- to centennial-scale palaeoclimatic variations during Termination I and the Holocene in the central Mediterranean Sea, *Global Planet. Change*, *40*, 201–217.
- Schilman, B., M. Bar Matthews, A. Almogi Labin, and B. Luz (2001), Global climate instability reflected by eastern Mediterranean marine records during the late Holocene, *Palaeogeogr. Palaeoclimatol. Palaeoecol.*, *176*, 157–176.
- Shindell, D. T., G. A. Schmidt, M. E. Mann, D. Rind, and A. Waple (2001), Solar forcing of regional climate change during the Maunder Minimum, *Science*, *294*, 2149–2152.
- Siani, G., M. Paterne, E. Michel, R. Sulpizio, A. Sbrana, M. Arnold, and G. Haddad (2001), Mediterranean sea surface radiocarbon reservoir age changes since the last glacial maximum, *Science*, *294*, 1917–1920.
- Suiver, M., P. J. Reimer, E. Bard, J. W. Beck, G. S. Burr, K. A. Hughen, B. Kromer, G. McCormac, J. Van Der Plicht, and M. Spurk (1998), INTCAL98 radiocarbon age calibration, 24,000–0 cal BP, *Radiocarbon*, *40*, 1041–1083.
- Thompson, D. W. J., and J. M. Wallace (2001), Regional climate impacts of the Northern Hemisphere annular mode, *Science*, *292*, 85–89.
- Turkes, M., and E. Erlat (2003), Precipitation changes and variability in Turkey linked to the North Atlantic Oscillation during the period 1930–2000., *Int. J. Climatol.*, *23*, 1771–1796.
- Visbeck, M., E. P. Chassignet, R. G. Curry, T. L. Delworth, R. R. Dickson, and G. Krahnmann (2003), The ocean's response to North Atlantic Oscillation variability, in *The North Atlantic Oscillation: Climatic Significance and Environmental Impact*, *Geophys. Monogr. Ser.*, vol. 134, edited by J. W. Hurrell et al., pp. 113–145, AGU, Washington, D. C.
- Zangvil, A., S. Karas, and A. Sasson (2003), Connection between eastern Mediterranean seasonal mean 500 hPa height and sea-level pressure patterns and the spatial rainfall distribution over Israel, *Int. J. Climatol.*, *23*, 1567–1576.

H. W. Arz and F. Lamy, GeoForschungs-Zentrum-Potsdam, Telegrafenberg, 14473 Potsdam, Germany. (flamy@gfz-potsdam.de)

A. Bahr and J. Pätzold, Fachbereich Geowissenschaften, Universität Bremen, Klagenfurter Strasse, 28259 Bremen, Germany.

G. C. Bond, Lamont-Doherty Earth Observatory of Columbia University, P.O. Box 1000, Palisades, NY 10964-8000, USA.